Modeling Resonances in Transmission Lines Fabricated Over Woven Fiber Substrates

Reydezel Torres-Torres, *Member, IEEE*, Gerardo Romo, Martin Schauer, *Member, IEEE*, Chudy Nwachukwu, *Student Member, IEEE*, and Seung-Won Baek

***Abstract*—This paper models transmission lines (TLs) fabricated over a printed circuit board substrate made of woven fiber fabric that causes resonances in the insertion and return loss. The modeling relies on the fact that these lines can be analyzed as periodically loaded TLs. Here, a method to determine the associated equivalent propagation constant and characteristic impedance is proposed. This allows to accurately reproduce the S-parameters for a TL of arbitrary length and for any periodicity of the fiber weave pattern along the line requiring neither multi-staged equivalent circuits, nor full-wave simulations.**

***Index Terms*—Fiber weave, interconnect, printed circuit board (PCB), resonances.**

I. Introduction

PRINTED circuit board (PCB) laminates are manufactured by impregnating and strengthening a woven fiberglass fabric with epoxy resin [1], a material that is anisotropic [2], [3]. In fact, when an interconnect fabricated on PCB is operated at a frequency (f) at which the wavelength (λ) of the propagating signal is comparable to the spacing between fibers, it can be treated as a periodically loaded transmission line (TL) [4]. In this case, these TLs exhibit stopband and passband characteristics. More precisely, at frequencies at which multiples of $\lambda/2$ equal the period of the fiber weave along the TL, resonances become apparent in the corresponding transmission and reflection responses. We proposed in recent publications full-wave models for representing this effect with success [5], [6], which allowed to understand the corresponding impact on the transmission and reflection properties of the lines. For circuit design, however, compact and equivalent-circuit models are preferred to ease and speed up simulations [7]. For this purpose, modeling the characteristics exhibited by a periodically loaded TL can be achieved using cascaded $ABCD$ matrices representing a single cell associated with each period of the TL [8]. Nevertheless, a considerable number of stages of this type might be required for representing the relatively long TLs used in packaging technologies even at operation frequencies of a few gigahertz, and the same constraint applies to directly using equivalent-circuit representations [9]. In addition, even though there are some attempts in the literature to obtain the equivalent propagation constant and characteristic impedance for a periodic TL around the frequency at which resonances occur [10], [11], until now there is no way to obtain these parameters directly from experimental data while simultaneously considering the inherent TL losses.

In [12], a hybrid approach combining the representation of a single cell using a 3D-model as in [5] and [6] and a single $ABCD$ matrix is presented to model periodically loaded PCB TLs. In this case, however, precise determination of the variations in the complex propagation constant and characteristic impedance along a period of TL is needed, which still involves discretional data correlation using a full-wave solver.

Here, a simple methodology to obtain the fundamental parameters of periodically loaded TLs directly from S-parameter measurements without requiring full-wave simulations is presented and demonstrated. Moreover, the methodology allows to model the resonances occurring at microwave frequencies in TLs fabricated in a commercially available PCB process when the metal traces are routed at different angles. This enables circuit designers to assess the impact of this undesired effect on the performance of practical PCB interconnects by a simple processing of experimental data.

II. Problem Statement

Fig. 1 shows a typical configuration in two dimensions of the fiberglass pattern for a PCB substrate. In this figure, the vertical and horizontal fiberglass bundles were denoted as the warp and weft yarns respectively, whereas the angle at which the metal trace runs over the substrate is measured from the latter. These definitions are used throughout this paper. It is well known that this type of anisotropic substrate results in a dependency of the electrical properties of the TLs running over it with respect to the angle Φ and position. This effect introduces a variation on the characteristic impedance (Z_c) and per-unit-length propagation constant (γ) from line to line [13]. A more serious problem, however, is that introduced by the glass-wave periodic loading of the line, which originates resonances that seriously affect the transmission and reflection characteristics of the TL. In [5], it was experimentally demonstrated that an accurate way to predict the lowest frequency at which a resonance due to the fiberglass pattern occurs $(f_{\rm res})$ is by using a very simple trigono-

Manuscript received February 08, 2013; revised April 22, 2013; accepted April 25, 2013. Date of publication May 20, 2013; date of current version June 28, 2013. This work was supported in part by CONACyT-Mexico under Grant 154337.

R. Torres-Torres is with the Instituto Nacional de Astrofísica, Óptica y Electrónica (INAOE), Department of Electronics, Tonantzintla, Puebla 72840, Mexico (e-mail: reydezel@inaoep.mx).

G. Romo is with Qualcomm Technology Inc., San Diego, CA 92121 USA (e-mail: gerardor@qti.qualcomm.com).

M. Schauer and S.-W. Baek are with CST of America, San Mateo, CA 94404 USA (e-mail:martin.schauer@cst.com).

C. Nwachukwu is with Gold Circuit Electronics, Santa Clara, CA 95054 USA (e-mail: CNwachukwu@gcegss.com).

Color versions of one or more of the figures in this paper are available online at http://ieeexplore.ieee.org.

Digital Object Identifier 10.1109/TMTT.2013.2261314

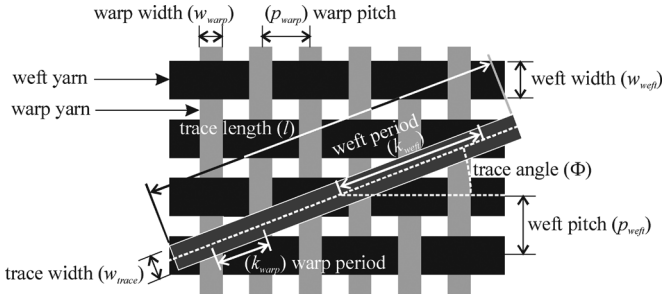

Fig. 1. Sketch showing a metal trace over a woven fiber substrate including the definition of some parameters used for the corresponding analysis.

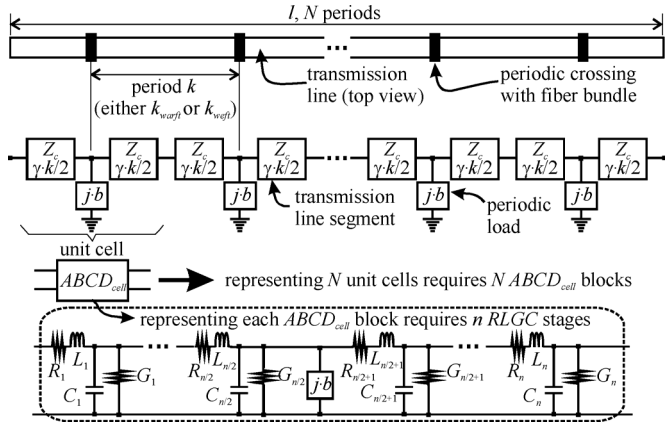

Fig. 2. Representation of a periodically loaded TL using two-port network blocks. Each $ABCD$ parameter block can be represented by means of $RLGC$ elements.

metric derived expression. This expression involves the geometric parameters defined in Fig. 1, and was simplified here to

$$f_{\mathrm{res}} = \frac{c \sin \Phi}{2p\sqrt{\varepsilon_{\mathrm{eff}}}} \tag{1}$$

where c is the speed of light, $\varepsilon_{\mathrm{eff}}$ is the effective relative permittivity of the TL environment, Φ is the trace angle, and p is the pitch of the fibers that yield the larger period along the TL (i.e., either p_{warp} or p_{weft}). Thus, from (1), it is possible to predict f_{res} with an error of less than 5% when p_{warp} or p_{weft} are measured between the middle point of the corresponding fiberglass bundles [5]. These periods (i.e., either k_{warp} or k_{weft}), depending on Φ, are in the order of some millimeters in current PCB technology, originating resonances at gigahertz frequencies.

In order to explain the way a periodically loaded TL is represented in circuit simulators, some concepts are reviewed hereafter.

A homogeneous TL can be represented by means of the corresponding per-unit-length $RLGC$ elements. From the theory in [14], for a specific length (l), the minimum number of $RLGC$ blocks (n) for accurately considering the distributed nature of the TL can be determined from

$$n = \Delta l|\gamma| \approx \Delta l\beta. \tag{2}$$

where Δ is an arbitrary constant typically set to 4 on PCB technologies, whereas for the sake of illustrating how many $RLGC$ blocks might be required to represent a TL on PCB, $|\gamma| \approx \beta$ was assumed. It is not uncommon to find that β presents values of hundreds of radians per meter in this type of interconnects when operating at some tens of gigahertz (reaching even more than 1000 rad/m beyond 40 GHz). Thus, in accordance with (2), hundreds of blocks are needed to represent each meter of TL, or tens of blocks per centimeter, being the latter an appropriate dimension to measure a TL on PCB. Unfortunately, including tens of $RLGC$ blocks in a circuit simulator might considerably increase the simulation time due to the large amount of interconnects included in a circuit design. Besides, the $RLGC$ parameters are dependent on f, making it necessary to implement sub-circuits for each element [15]. For this reason, alternatively, in some simulators it is possible to represent the TL directly using the $ABCD$-parameter equivalent representation given by

$$ABCD = \begin{bmatrix} A & B \\ C & D \end{bmatrix} = \begin{bmatrix} \cosh(\gamma l) & Z_c \sinh(\gamma l) \\ \frac{\sinh(\gamma l)}{Z_c} & \cosh(\gamma l) \end{bmatrix}. \tag{3}$$

Thus, independently of the length of the TL, (3) allows the determination of the corresponding transmission and reflection characteristics from a single matrix computation.

Analogously, the previous discussion can be extended to a periodically loaded TL. In this case, the TL depicted in Fig. 1 can be seen as the periodically loaded TL shown at the top of Fig. 2. In accordance to [8], each one of the periodic loads experienced by the TL can be modeled by means of a shunt admittance $j \cdot b$ (where $j^2 = -1$), and the line can be divided into N cells, where N is the number of loads present along the line. In fact, since the periodically loaded TL behaves basically as a homogeneous TL, except around the frequencies at which resonance occurs, each unit cell in Fig. 2 is composed of a shunt load admittance embedded between two sections of homogeneous TL. These sections equal $l = k/2$ since each cell represents a period of length k. Notice that using this approach would require tens of cells for a TL of some centimeters fabricated on PCB.

Continuing the analysis, by applying two-port network theory, the $ABCD$ matrix of each unit cell in Fig. 2 can be obtained as [8]

$$\begin{aligned} ABCD_{\mathrm{cell}} &= \begin{bmatrix} A_{\mathrm{cell}} & B_{\mathrm{cell}} \\ C_{\mathrm{cell}} & D_{\mathrm{cell}} \end{bmatrix} \\ &= ABCD_{l=\frac{k}{2}} \begin{bmatrix} 1 & 0 \\ jb & 1 \end{bmatrix} ABCD_{l=\frac{k}{2}} \\ &= \begin{bmatrix} \cosh(\gamma k) + j\frac{bZ_c \sinh(\gamma k)}{2} & Z_c \sinh(\gamma k) - j\frac{bZ_c^2[\cosh(\gamma k)-1]}{2} \\ \frac{\sinh(\gamma k)}{Z_c} - j\frac{b[\cosh(\gamma k)-1]}{2} & \cosh(\gamma k) + j\frac{bZ_c \sinh(\gamma k)}{2} \end{bmatrix}. \end{aligned} \tag{4}$$

Observe that (4) represents a unit cell and still the cascade connection of N stages for modeling a complete TL line is required. Furthermore, in case that an equivalent-circuit model is required for the periodically loaded TL, the number of $RLGC$ stages within the unit cell has to be determined by substituting l in (2) for the period of the loads considering β for the maximum f of operation of the line. In this case, hundreds of $RLGC$ stages would be required in total for a line of a few centimeters. Thus, in the following section, a matrix for representing a

periodically loaded TL of arbitrary periodicity of the load and featuring any length is presented.

III. Model Parameter Determination

This paper is dedicated to finding the equivalent complex propagation constant (γ_p) and characteristic impedance (Z_p) as a function of f for a periodically loaded TL. For this purpose, the following analysis is carried out. Similarly to the case of a homogeneous TL, it is possible to define the following matrix for a periodically loaded TL

$$ABCD_p = \begin{bmatrix} A_p & B_p \\ C_p & D_p \end{bmatrix} = \begin{bmatrix} \cosh(\gamma_p l) & Z_p \sinh(\gamma_p l) \\ \frac{\sinh(\gamma_p l)}{Z_p} & \cosh(\gamma_p l) \end{bmatrix} \quad (5)$$

where $\gamma_p = u + jv$ and $Z_p = R_p + jI_p$. Notice that, in contrast to (4), (5) represents a TL of any length l containing an arbitrary number of periodical loads.

The real and imaginary parts of A_p in (5) can be written, respectively, as

$$\mathrm{Re}(A_p) = \cosh(ul)\cos(vl) \quad (6)$$

$$\mathrm{Im}(A_p) = \sinh(ul)\sin(vl). \quad (7)$$

Since the unit cell depicted in Fig. 2 can be represented by (5) provided that $l = k$, for this particular case, A_p can be written in terms of $\gamma = \alpha + j\beta$, $Z_c = R_c + jI_c$, and b when equating (5) to (4). This yields the following alternative expressions for the real and imaginary parts of A_p:

$$\mathrm{Re}(A_p) = \cosh(\alpha k)\cos(\beta k) - \frac{b\left[I_c \sinh(\alpha k)\cos(\beta k) + R_c \cosh(\alpha k)\sin(\beta k)\right]}{2} \quad (8)$$

$$\mathrm{Im}(A_p) = \sinh(\alpha k)\sin(\beta k) + \frac{b\left[R_c \sinh(\alpha k)\cos(\beta k) - I_c \cosh(\alpha k)\sin(\beta k)\right]}{2}. \quad (9)$$

At the moment, assume that γ, Z_c, b, and k are known within the f-bandwidth of interest. In this case, the complex value of A_p can be obtained from (8) and (9), and for simplicity, the results are defined as $\mathrm{Re}(A_p) = R_A$ and $\mathrm{Im}(A_p) = I_A$. Thus, using these results and assuming $l = k$, it is possible to equate R_A to (6) and I_A to (7), which yields

$$R_A = \cosh(u\,k)\cos(v\,k) \quad (10)$$

$$I_A = \sinh(u\,k)\sin(v\,k). \quad (11)$$

Attempting to directly solve the previous system of nonlinear equations yields complicated results with multiple roots that are difficult to discriminate to obtain u and v. Thus, additional analysis is required as shown hereafter.

Using trigonometric identities, it is possible to rewrite (10) and (11) as

$$R_A^2 = (1 + x)(1 - y) \quad (12)$$

$$I_A^2 = xy \quad (13)$$

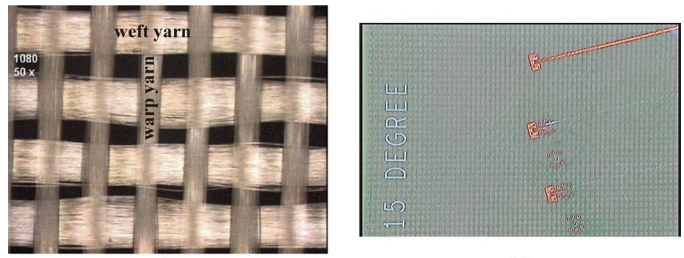

a) b)

Fig. 3. Photographs showing: (a) the fiberglass pattern of the substrate used to implement the prototype and (b) partial view of the PCB prototype showing the termination of a microstrip line on top.

where $x = \sinh^2(uk)$ and $y = \sin^2(vk)$. In this system of equations, y can be found by solving

$$y^2 + \left(R_A^2 + I_A^2 - 1\right) y - I_A^2 = 0. \quad (14)$$

Only one of the two roots for (14) yields a positive value for y that results in the form of a sine-squared function when plotted versus f. This root corresponds to $\sin^2(vk)$, from where v can be easily obtained. Once v is known, u can be found from (11), which completes the determination of γ_p.

For the case of Z_p, the corresponding complex value can be obtained from B_p after substituting $l = k$ and the determined values for γ_p in (5); mathematically,

$$Z_p = \frac{B_p}{\sinh(\gamma_p k)}. \quad (15)$$

Notice that the procedure proposed in this section, unlike the simplified approach studied in textbooks [8], takes into account the losses occurring along the periodically loaded TL. This is achieved by simultaneously considering the complex γ and Z_c values without significantly increasing the complexity of the resulting equations.

IV. Prototypes and Experiments

For verifying the proposal, it is convenient to analyze experimental data corresponding to periodically loaded TLs implemented on a PCB substrate in which the fiberglass pattern is comparable with the wavelength of the propagated signal. Moreover, to show that the proposal is useful in current applications, the substrate in these experiments meets the specifications of the IS680 material that uses a type-1080 glass style manufactured by the Isola Group. This material presents small relative permittivity and dissipation factor, which makes it a suitable substrate for high-frequency PCBs.

The substrate was carefully constructed with one ply of glass fabric as that shown in Fig. 3(a), where the weft and warp yarns are made of the same material presenting nominal relative permittivity and loss tangent of 4.8 and 0.003, respectively. The nominal dimensions of the resulting pattern are $p_{\mathrm{weft}} = 600\ \mu$m, $w_{\mathrm{weft}} = 350\ \mu$m, $p_{\mathrm{warp}} = 400\ \mu$m, and $w_{\mathrm{warp}} = 200\ \mu$m. This fabric was impregnated with a specific resin content to ensure an adequate amount of buttercoat (i.e., un-reinforced resin) after press lamination. This is important because insufficient buttercoat might lead to severe glass stop

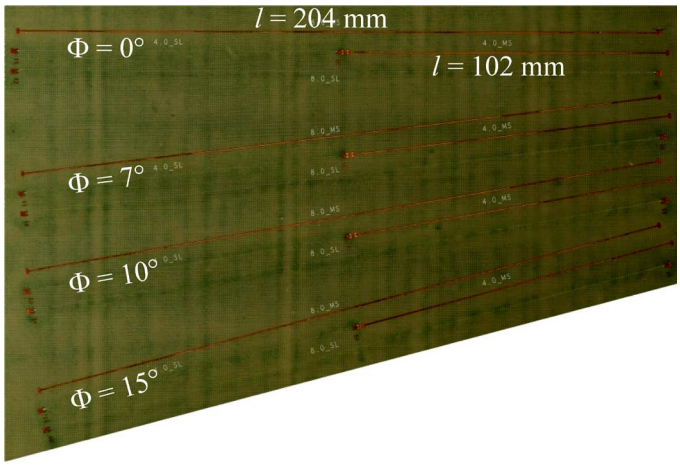

Fig. 4. Photograph showing the microstrip lines at different angles (increasing Φ from top to bottom). Notice that two lines of different lengths are fabricated for each angle.

where the conductor traces press up directly against the weave fabric. Otherwise, the glass stop can significantly affect the trace impedance and ultimately the electrical performance of the laminate material. This is not desirable for the experiments here since it is important that the fabricated lines present the same cross-sectional dimensions along the signal propagation direction to ensure that the periodic loading is only due to variations on the dielectric properties of the substrate.

Regarding the metal layers, these are made of copper deposited by means of an industry standard electroplating process. In this case, the thickness of the resulting layers is 18 μm, whereas the metal–dielectric interface presents a root mean square roughness of 670 nm.

The substrate is thus a composite of one ply of weave fabric impregnated with 72% resin content to obtain a thickness of 100 μm. However, the thickness of the prepreg material is reduced to approximately 86 μm after etched areas of copper are filled by flowing resin during lamination. In this substrate, microstrip lines designed to present $Z_c \approx 50\ \Omega$ were etched at different Φ angles, as defined in Fig. 1, so that k_{weft} is different in each case and the corresponding resonances occur at different frequencies. These lines present $w_{\mathrm{trace}} = 240\ \mu$m, and experience an approximate effective permittivity and loss tangent of 2.45 and 0.002, respectively. These parameters were experimentally determined from S-parameter measurements at 10 GHz and present variations of less than $\pm 1\%$ for the different considered Φ angles.

Moreover, in order to obtain γ and Z_c from experimental S-parameters using a line-line procedure, TLs of two different lengths (i.e., $l = 102$ mm and 204 mm) at each one of the considered angles are fabricated. Fig. 4 shows a photograph of the finished prototype. For these lines, k_{weft} and the corresponding f_{res}, as calculated from (1), are summarized in Table I. This table also includes the number of periods (i.e., the number of admittance loads) present in the fabricated microstrip lines with $l = 102$ mm. The later information is useful to determine the number of unit cells required for the corresponding equivalent circuit model that will be used for comparison of results. Notice that for the TL with $\Phi = 0°$, no resonance is considered since the trace runs in parallel with the weft yarn, whereas the weft period is too small to originate resonances within the range of frequencies of interest in this paper.

TABLE I
CALCULATED WEFT PERIOD, NUMBER OF PERIODS FOR A LINE WITH $l = 102$ mm, AND RESONANCE FREQUENCY FOR THE FABRICATED MICROSTRIP LINES

Φ	$k_{weft} = p_{weft}/\sin(\Phi)$ (mm)	N ($l = 102$ mm)	f_{res} (GHz)
15°	2.3	44	41.3
10°	3.5	29	27.7
7°	4.9	21	19.5
0°	-	-	-

The fabricated microstrip lines were terminated with ground–signal–ground configured pads so that S-parameters are measured using coplanar RF probes with a pitch of 250 μm [see Fig. 3(b)]. For this purpose, a vector network analyzer (VNA) was used by defining a measurement span for f from 10 MHz to 50 GHz. The measurement setup was calibrated up to the probe tips by using a line–reflect–match (LRM) algorithm and an impedance standard substrate (ISS) provided by the probe manufacturer, which also allowed to establish a reference impedance of 50 Ω. Afterwards, γ was determined from the experimental data of every pair of TLs with common Φ by applying a line–line procedure that removes the effect of the parasitics associated with the pads [16]. For the case of Z_c, the experimental determination is carried out from γ using the procedure described in [17].

V. RESULTS AND DISCUSSION

The most common way to experimentally obtain γ and Z_c is using line–line algorithms [16] requiring the S-parameter measurements of two lines presenting identical measurement terminations, different lengths, and the same cross section along the direction of propagation. This method, however, also requires that single-mode propagation occurs in the lines within the f-range where the extraction is performed. Note that this condition is not satisfied in a periodically loaded TL at frequencies around f_{res} due to the presence of evanecent waves. Thus, when this method is applied to periodically loaded TLs, some fluctuations are expected in γ and Z_c near the resonance frequencies. This fact has been previously verified through full-wave simulations of TLs in woven fiber substrates [5], also showing that an electromagnetic bandgap is observed in a dispersion diagram, corresponding to the frequency range of evanescent modes [6].

Fig. 5 shows γ and Z_c obtained from experimental data to the fabricated lines. Notice that these curves do not significantly change for the fabricated TLs when varying Φ, except around the frequencies at which resonances are expected to occur as predicted by (1). In fact, the results for the lines with $\Phi \neq 0$ are particularly noisy around f_{res} since, as mentioned above, the line–line algorithm fails when evanescent waves are present. For the case of Z_c, the extraction was carried out from a calculation involving γ, the capacitance of the lines at a low f, and the effective loss tangent [17]. Thus, the error in the determination of γ using the line–line procedure around f_{res} is also reflected in the data obtained for Z_c. For this reason, for periodically loaded

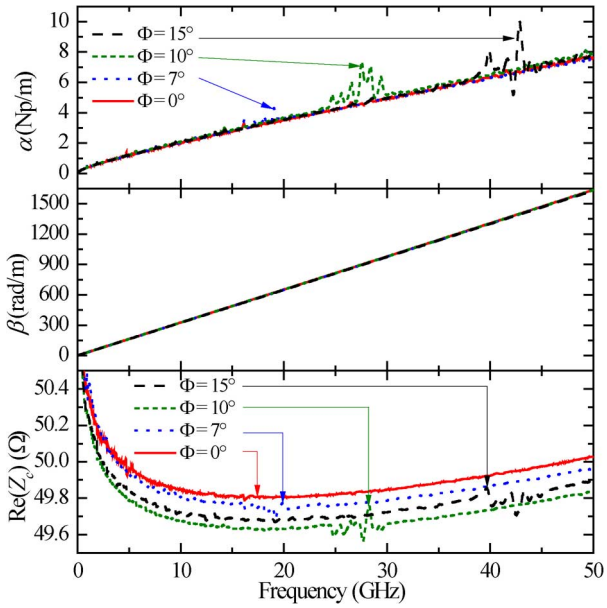

Fig. 5. Propagation constant and characteristic impedance determined from experimental data. For the lines with $\Phi \neq 0$, the line–line method fails and yields large fluctuations in the extracted data around $f_{\rm res}$.

TLs, applying the parameter extraction described in Section III is preferable in order to obtain the corresponding effective propagation constant and characteristic impedance.

In order to apply and verify the proposed method, R_A and I_A need to be determined from (8) and (9) in the frequency range and for the lines of interest. These equations require α, β, R_c, I_c, k, and b. From these parameters, α, β, R_c, and I_c, represent the homogeneous sections of TL composing the unit cell in Fig. 2. They can be obtained from γ and Z_c corresponding to the TL with $\Phi = 0°$ (i.e., in this TL, no resonances are present within the measured frequency range). Furthermore, k corresponds to $k_{\rm weft}$ in the fabricated lines since the longest period, which originates the lowest $f_{\rm res}$, is associated with the crossing of the metal trace with the weft yarn (see Fig. 1). Thus, $k = k_{\rm weft}$ can be obtained as in Table I once $p_{\rm weft}$ is known. Note that this parameter defines the frequency at which the resonance occurs. In case that a visual inspection of the sample is not possible, $p_{\rm weft}$ can be found by solving (1) for a specific value of $f_{\rm res}$ (e.g., observed in the experimental $|S_{21}|$ versus f data). At this point, the only unknown parameter for applying (8) and (9) is b, which presents the form of a capacitive susceptance ωC_b [9], [18], where $\omega = 2\pi f$ and C_b is determined through the model-experiment correlation explained hereafter.

C_b determines the magnitude of the resonance. Hence, when assuming $b = j\,\omega C_b = 0$ in (8) and (9), solving (14) and (15) yields $\gamma_p = \gamma$ and $Z_p = Z_c$ since the periodic load is ignored. Conversely, when increasing the value of C_b, the magnitude of the resonance at $f = f_{\rm res}$ also increases, which affects the value of γ_p and Z_p around this frequency. Therefore, S-parameter simulations can be performed by substituting the obtained γ_p and Z_p in (5) for a given value of C_b and using the total length l of the TL to be modeled. In this case, γ_p and Z_p can be iteratively calculated by varying C_b until the simulated S-parameters correspond to the experimental data around

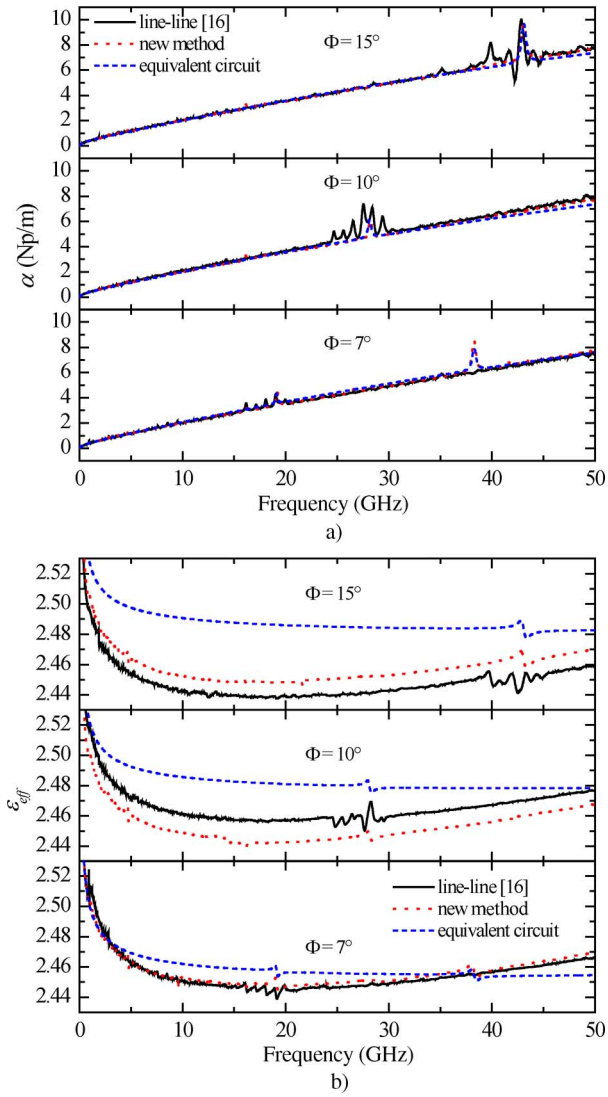

Fig. 6. Comparison of the: (a) attenuation and (b) $\varepsilon_{\rm eff}$ versus f curves using the line–line algorithm, the proposed approach, and the multi-stage equivalent circuit for lines with different Φ and $l = 102$ mm.

$f_{\rm res}$. Carrying out this procedure for obtaining C_b is fast since the quadratic equation given in (14) is the most complicated to solve. For $\Phi = 7°, 10°$, and $15°$, it is found that $C_b = 4$ fF, 3 fF, and 2.3 fF, respectively. This is an expected result since as Φ increases, the overlap between the metal trace and the weft yarn becomes smaller (see Fig. 1), reducing the magnitude of the discontinuity and yielding a smaller value for C_b in the model.

Before showing the obtained results, it is worthwhile to mention that at this point it is possible to represent TLs of any length at the considered angles using (5). For comparison purposes, however, the equivalent-circuit model shown in Fig. 2 is implemented for the TLs with $l = 102$ mm and different Φ. In this case, different number of periods are encountered for the fabricated TLs, as detailed in Table I. For instance, for $\Phi = 15°$, the number of unit cells required to implement the model is $N = 44$. Since each unit cell represents a section of TL with length $k_{\rm weft} = 2.3$ mm, using (2) and the curve for β in Fig. 5, the number of $RLGC$ stages to represent this section is $n = 14$ in order to cover an f range up to 50 GHz. This yields a total

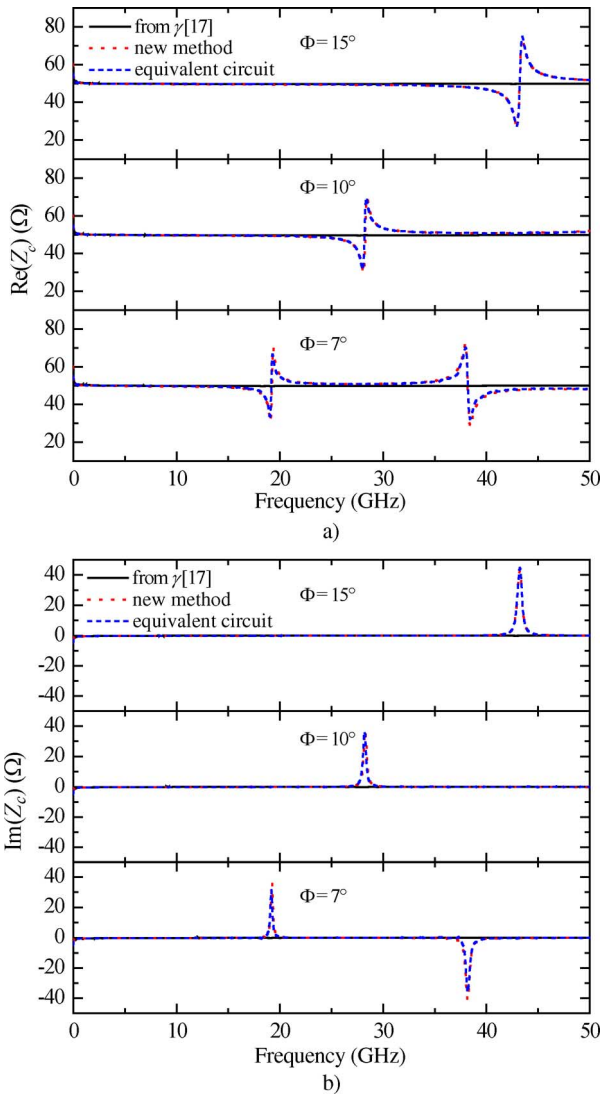

Fig. 7. Comparison of the: (a) real part and (b) imaginary part of the characteristic impedance versus f curves obtained directly using γ, by applying the proposed approach, and with the multi-stage equivalent circuit for lines with different Φ and $l = 102$ mm.

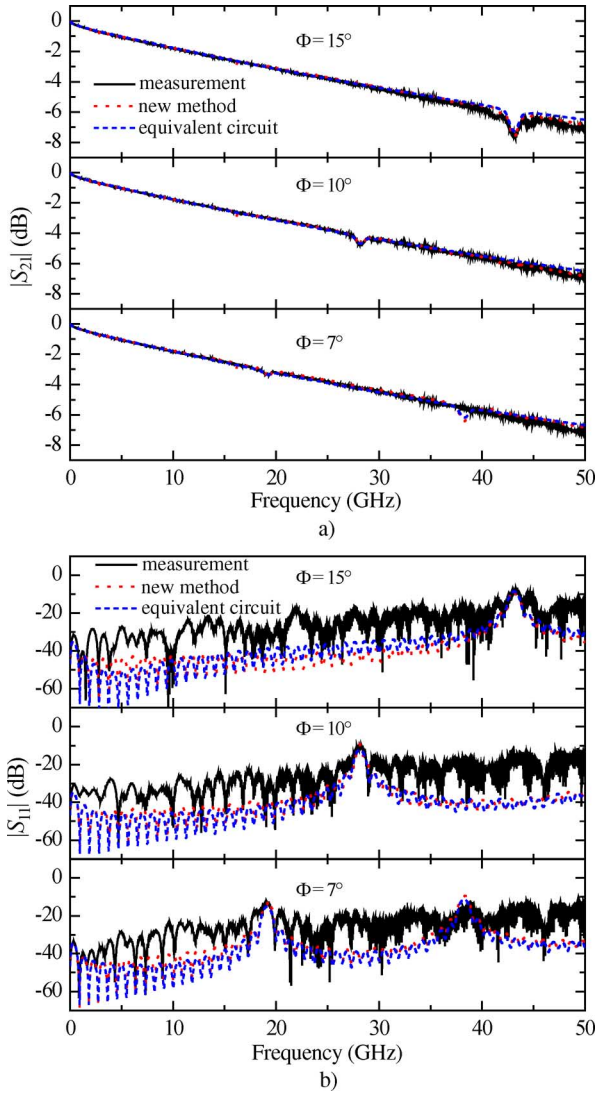

Fig. 8. Comparison of the: (a) insertion and (b) return loss versus f curves obtained from measurements, by applying the proposed approach, and with the multi-stage equivalent circuit for lines with different Φ and $l = 102$ mm.

of $N \cdot n = 616$ $RLGC$ stages to represent the complete TL. Bear in mind that the $RLGC$ elements are dependent on f, and sub-networks might be required to represent these elements in case that the available circuit simulator only accepts constant values for lumped $RLGC$ components [15].

Fig. 6(a) shows the attenuation versus f data obtained by applying the proposed approach for lines with different Φ and $l = 102$ mm. Notice that the frequencies of resonance for each line are in agreement with those listed in Table I. This is also achieved when processing data obtained using the implemented equivalent circuit, but substantially increasing the complexity of the simulations. On the other hand, the data obtained directly by applying the line–line algorithm to lines with $\Phi \neq 0°$ gives an idea of the value for f_{res}. Nevertheless, very noisy data are obtained around f_{res} since the method fails when no single mode propagation is taking place. Conversely, the curves obtained with the proposed approach allow to obtain physically expected results (e.g., α considerably increases around f_{res}) in a very simple and direct way. Besides, instead of plotting β versus f, Fig. 6(b) shows $\varepsilon_{\text{eff}} = (c\beta/\omega)^{0.5}$ versus f curves since the large and monotonically increasing β versus f curves do not allow to observe resonances. In contrast, the curves in Fig. 6(b) clearly exhibit resonances at the same points as those obtained for the attenuation.

An interesting observation in Fig. 6(a) is the fact that even though the overlap between the metal trace and the weft yarn decreases as Φ increases, the TL experiences more periods in this case, resulting in an increased magnitude of α around f_{res} as Φ increases. In other words, as expected, the attenuation within the rejection band is higher as the number of periods along the TL increases. In addition, notice that for the simulated curves corresponding to $\Phi = 7°$, a second resonance at $f = 2f_{\text{res}}$ is observed since this effect occurs at submultiples of half the signal wavelength. Nevertheless, the experimental curves do not show this second resonance due to the poor Q factor exhibited by the TL at this frequency considering the relatively low magnitude of the rejection for this line. Further analysis to quantify

the magnitude of this second resonance can be carried out involving the Q factor of the TL when the associated metal and dielectric losses are appropriately determined [19].

Fig. 7 compares Z_p determined using three different approaches: after applying [17] to experimental data, from equivalent-circuit simulations, and applying the proposed method. For the case of the method in [17], the resonances are not apparent since the corresponding curves are obtained from an experimental data fitting that assumes single TEM-mode propagation. For the curves obtained using the equivalent-circuit model, the simulated S-parameters were transformed to $ABCD$ parameters, which are assumed to present the form shown in (5). Thus, from these data, it is possible to calculate $Z_p = (B_p/C_p)^{0.5}$ and plot the resulting curves as a function of f in Fig. 5. When comparing these curves with those obtained using the proposed (15), the agreement is excellent, while there is also agreement with the characteristic impedance obtained as in [17], except around $f_{\rm res}$.

Once γ_p and Z_p are known, it is possible to calculate the $ABCD$ parameters of a TL using (5) and then obtaining the corresponding S-parameters using a simple two-port parameter transformation. In addition, for comparison purposes, the S-parameters are directly obtained from simulations performed to an equivalent circuit. These curves are compared with measurements in Fig. 8 for lines with different Φ. The resonances are predicted with accuracy using both the equivalent circuit and the proposed method. Using the later is considerably simpler.

VI. Conclusions

Resonances in TLs fabricated over woven fiber substrates are apparent at microwave frequencies for current fabrication technologies. The work presented here contributes to the analysis of this undesired effect by providing a model and parameter-extraction methodology that accurately represent the magnitude and frequency of occurrence of these resonances. The parameter-extraction method relies on the fact that interconnects over this type of substrate can be considered as TLs periodically loaded with shunt capacitive susceptances. This eases the analysis and allows a simple model implementation using only S-parameter measurements.

References

[1] S. Rzepka, F. Krämer, O. Grassmé, and J. Lienig, "A multilayer PCB material modeling approach based on laminate theory," in *Proc. EuroSimE*, Freiburg-im-Breisgau, Germany, Apr. 2008, pp. 1–10.

[2] M. S. Mirotznik, S. Yarlagadda, R. McCauley, and P. Pa, "Broadband electromagnetic modeling of woven fabric composites," *IEEE Trans. Microw. Theory Techn.*, vol. 60, no. 1, pp. 158–169, Jan. 2012.

[3] M. Y. Koledintseva, J. L. Drewniak, and S. Hinaga, "Effect of anisotropy on extracted dielectric properties of PCB laminate dielectrics," in *Proc. IEEE Int. EMC Symp.*, Long Beach, CA, USA, Aug. 2011, pp. 514–517.

[4] J. R. Miller, G. J. Blando, and I. Novak, "Additional trace losses due to glass-weave periodic loading," in *Proc. DesignCon*, Santa Clara, CA, USA, Feb. 2010, pp. 799–821.

[5] G. Romo, C. Nwachukwu, R. Torres-Torres, S.-W. Baek, and M. Schauer, "Stack-up and routing optimization by understanding micro-scale PCB effects," in *Proc. DesignCon*, Santa Clara, CA, USA, Feb. 2011, pp. 758–782.

[6] M. Schauer, G. Romo, R. Torres-Torres, C. Nwachukwu, and S.-W. Baek, "Understanding and mitigation of fiber weave effects in striplines," in *Proc. DesignCon*, Santa Clara, CA, USA, Feb. 2012, pp. 664–688.

[7] L. Simonovich, "Practical fiber weave effect modeling," Lamsim Enterprises, Stittsville, ON, Canada, White Paper, 2011.

[8] D. M. Pozar, *Microwave Engineering*. New York, NY, USA: Wiley, 2005.

[9] N. Yang and Z. N. Chen, "Microstrip line periodic structures with capacitive and resonant element loads," in *Proc. IWAT*, Singapore, Mar. 2005, pp. 391–394.

[10] L. Zhu, "Guided-wave characteristics of periodic coplanar waveguides with inductive loading—Unit-length transmission parameters," *IEEE Trans. Microw. Theory Techn.*, vol. 51, no. 10, pp. 2133–2138, Oct. 2003.

[11] E. Takagi, "Frequency dependence of Bloch impedance in a periodic transmission line structure," in *IEEE MTT-S Int. Microw. Symp. Dig.*, Phoenix, AZ, USA, May 2001, vol. 2, pp. 779–782.

[12] P. Pathmanathan, P. G. Huray, and S. G. Pytel, "Analytic solutions for periodically loaded transmission line modeling," in *Proc. DesignCon*, Santa Clara, CA, USA, Feb. 2013, pp. 1–22.

[13] S. Hall and H. Heck, *Advanced Signal Integrity for High-Speed Digital Designs*. Hoboken, NJ, USA: Wiley, 2009.

[14] H. Johnson and M. Graham, *High-Speed Signal Propagation: Advanced Black Magic*. Upper Saddle River, NJ, USA: Prentice-Hall, 2003.

[15] A. Schellmanns, J. Keradec, and J. Schanen, "Electrical equivalent circuit for frequency dependant impedance: Minimum lumped elements for a given precision," in *Ind. Appl. Conf.*, Oct. 2000, vol. 5, pp. 3105–3115.

[16] J. A. Reynoso-Hernández, "Unified method for determining the complex propagation constant of reflecting and nonreflecting transmission lines," *IEEE Microw. Wireless Compon. Lett.*, vol. 13, no. 8, pp. 351–353, Aug. 2003.

[17] R. Torres-Torres, "Extracting characteristic impedance in low-loss substrates," *Electron. Lett.*, vol. 47, no. 3, pp. 191–193, Feb. 2011.

[18] M. Y. Koledintseva, S. K. Patil, R. W. Schwartz, W. Huebner, K. Rozanov, J. Shen, and J. Chen, "Prediction of effective permittivity of diphasic dielectrics as a function of frequency," *IEEE Trans. Dielectr. Electr. Insul.*, vol. 16, no. 3, pp. 793–808, Jun. 2009.

[19] A. Koul, M. Y. Koledintseva, S. Hinaga, and J. L. Drewniak, "Differential extrapolation method for separating dielectric and rough conductor losses in printed circuit boards," *IEEE Trans. Electromagn. Compat.*, vol. 54, no. 4, pp. 421–433, Apr. 2012.

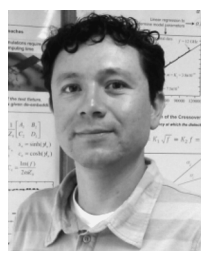

Reydezel Torres-Torres (S'01–M'06) received the Ph.D. degree from the Instituto Nacional de Astrofísica, Óptica y Electrónica (INAOE), Tonantzintla, Puebla, Mexico.

He is currently a Senior Researcher with the Microwave Research Group, INAOE. He was with Intel Laboratories, Guadalajara, Mexico, and IMEC, Heverlee, Belgium. He has authored over 40 journal and conference papers. He has directed three Ph.D. and six M.S. theses, all in experimental high-frequency characterization and modeling of materials, interconnects, and devices for microwave applications.

Gerardo Romo received the M.A.Sc. and Ph.D. degrees in electrical engineering from Carleton University, Ottawa, ON, Canada, in 2001 and 2005, respectively.

From 2005 to 2008, he was a Senior Hardware Engineer with the Systems Research Center of Intel, Guadalajara, Mexico, where he was involved with research and development of high-speed interconnects and electronic packages. His main research focused on exploring alternative technologies for high-speed interconnects such as substrate integrated waveguides. From 2009 to 2011, he was with CST of America, as a Senior Application Engineer with an emphasis on signal and power integrity applications. In August 2011, he joined the Power and Signal Integrity Group, Qualcomm Technology Inc., San Diego, CA, USA, where he is currently a Staff Engineer. His main interests are signal/power integrity and computational electromagnetics applied to high-frequency problems.

Martin Schauer (A'05–M'06) received the Dipl.-Ing. and Ph.D. degrees in electrical engineering from the Technische Universität Darmstadt, Darmstadt, Germany, in 1999 and 2005, respectively.

Since 1999, he has been with Computer Simulation Technology (CST), where he developed 3-D electromagnetic simulation software until 2005. He is currently an Engineering Manager for the western region of CST of America, San Mateo, CA, USA. His main interests are numerical methods and their application toward low- and high-frequency electromagnetic problems.

Chudy Nwachukwu (S'08) received the M.S.E.E. degree from Saint Cloud State University, Saint Cloud, MN, USA, in 2009. His graduate thesis on design optimization of components in high-speed PCBs was published.

He is currently a Member of Technical Staff and Account Manager with Gold Circuit Electronics, Santa Clara, CA, USA. He was a Signal Integrity and Application Development Engineer responsible for the design of test vehicles and engineering applications to meet the requirements of OEMs in the high-speed digital market. His background has focused on 3-D electromagnetic (EM) simulations and signal integrity analysis of line card and backplane channels.

Seung-Won Baek is currently an Application Engineer with CST of America, San Mateo, CA, USA. He was with LG Electronics, Korea MicroWave (KMW), and the Korea Basic Science Institute (KBSI). His previous experiences include a variety of vacuum tubes, appliances, and RF component design. He holds 14 international patents and 16 domestic patents on vacuum tubes.